
AMORTIZED LEARNING OF DYNAMIC FEATURE SCALING FOR IMAGE SEGMENTATION

Jose Javier Gonzalez Ortiz*
MIT CSAIL
josejg@mit.edu

John Guttag
MIT CSAIL
gutttag@mit.edu

Adrian V. Dalca
MGH, HMS and MIT CSAIL
adalca@mit.edu

ABSTRACT

Convolutional neural networks (CNN) have become the predominant model for image segmentation tasks. Most CNN segmentation architectures resize spatial dimensions by a fixed factor of two to aggregate spatial context. Recent work has explored using other resizing factors to improve model accuracy for specific applications. However, finding the appropriate rescaling factor most often involves training a separate network for many different factors and comparing the performance of each model. The computational burden of these models means that in practice it is rarely done, and when done only a few different scaling factors are considered.

In this work, we present a hypernetwork strategy that can be used to easily and rapidly generate the Pareto frontier for the trade-off between accuracy and efficiency as the rescaling factor varies. We show how to train a *single* hypernetwork that generates CNN parameters conditioned on a rescaling factor. This enables a user to quickly choose a rescaling factor that appropriately balances accuracy and computational efficiency for their particular needs. We focus on image segmentation tasks, and demonstrate the value of this approach across various domains. We also find that, for a given rescaling factor, our single hypernetwork outperforms CNNs trained with fixed rescaling factors.

Keywords Amortized Learning, Image Segmentation, Convolutional Neural Networks, Hypernetworks, Resizing

1 Introduction

Convolutional Neural Networks (CNNs) have become ubiquitous in computer vision [37]. Driven by the availability of massive datasets, popular models use large numbers of parameters to exploit the growing amount of information [23, 66]. These models require large amounts of computation, most often necessitating hardware accelerators like GPUs or TPUs for training and inference [36]. The computational burden at training time increases infrastructure costs and at inference time it limits deployment, specially in resource-constrained applications [64, 71]. In turn, the increase in computation induced by large machine learning models leads to increased energy requirements whose associated carbon emissions have a considerable environmental impact [53].

These concerns have led researchers to explore a variety of techniques for minimizing computational requirements while maintaining accuracy. Common strategies include quantization [27, 32, 56], pruning [6, 17, 20, 34], and factoring [10, 33, 70], which focus on reducing the parameter count and the size of the convolutional kernels. These methods usually introduce a trade-off between model accuracy and efficiency and require training multiple models in order to select the best model based on considerations regarding both metrics. These strategies do not explore reducing the spatial dimensions of the inputs to convolutional layers as a way to reduce the cost of convolutions.

Most modern CNN architectures repeatedly reduce the spatial scale of the features in their architectures by using spatial pooling operations such as max-pooling or strided convolutions. In practice, most network designs downscale by a factor of two [23, 26, 40, 66], without considering other possibilities. This can be inefficient, since the amount of rescaling of intermediate features plays a major role in network efficiency, because the cost of convolution operations is proportional to the spatial dimensions of the input feature maps.

*Corresponding author

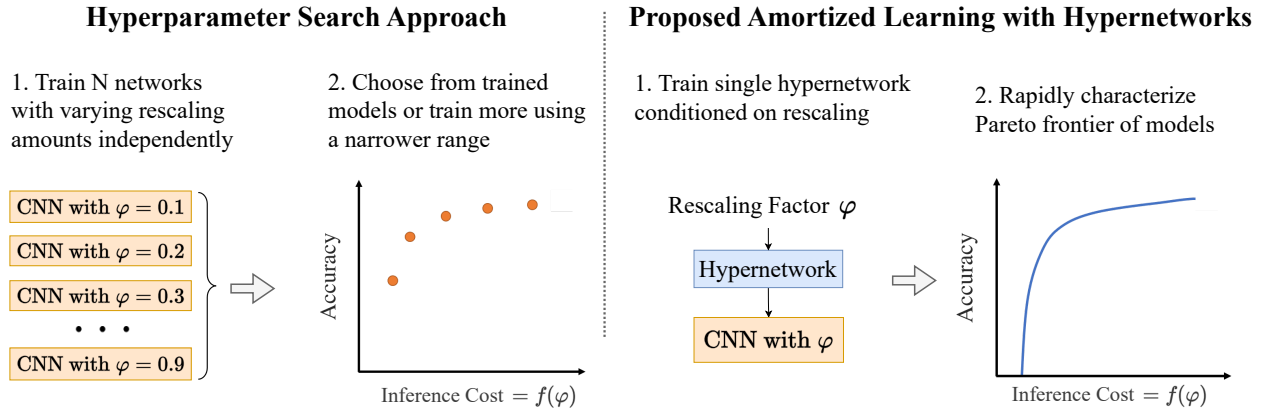


Figure 1: Strategies for exploring the accuracy-efficiency trade-off of varying the CNN rescaling factor. A standard approach (*left*) requires training N models with different rescaling factors independently. Our proposed amortized learning strategy (*right*) exploits the similarity between the tasks and trains a single hypernetwork model. Once trained, we can rapidly evaluate many rescaling settings and efficiently characterize the Pareto frontier between segmentation accuracy and computational cost for each dataset or task of interest. This enables rapid and precise model choices depending on the desired trade-off at inference.

Some research does explore alternative rescaling strategies [18, 42, 43, 72, 74] or very recently optimizing the rescaling layers as part of training [35, 45, 57]. However, these techniques either do not explore multiple rescaling factors, or jointly optimize the amount of rescaling while training for a fixed, pre-defined metric. Such approaches do not fully characterize the trade-off between model accuracy and the amount of rescaling performed in rescaling layers.

In this work, we propose an alternative approach. We show how to train a single hypernetwork that captures a complete landscape of models covering a continuous range of rescaling ratios. Once trained, the hypernetwork rapidly predicts model weights for an inference network for a desired rescaling factor. This predicted network is as efficient at inference as a regular network trained for a single rescaling factor. Training the hypernetwork requires scarcely more computation than training a model for a single rescaling factor, leading to a substantial improvement compared to training many standard models. Moreover, somewhat surprisingly, we find that its accuracy is typically better than that of a network trained with a single fixed rescaling factor. Our hypernetwork model can be used to rapidly generate the Pareto frontier for the trade-off between accuracy and efficiency as a function of the rescaling factor (Figure 1). This enables a user to choose, depending upon the situation, a rescaling factor that appropriately balances accuracy and computational efficiency.

We are motivated by the prevalent task of semantic segmentation, and evaluate the proposed method on semantic segmentation tasks on both natural images and medical brain scans. In our experiments, we find that a wide range of rescaling factors achieve similar accuracy results despite having substantially different inference costs. We demonstrate that the proposed hypernetwork based approach is able to learn models for a wide range of feature rescaling factors, and that inference networks derived from the hypernetwork perform at least as well, and in most cases better than, networks trained with fixed rescaling factors.

Our main contributions are:

- We introduce a hypernetwork model that, given a rescaling factor, generates the weights for a segmentation network that uses that amount of rescaling in the rescaling layers.
- We show that our approach makes it possible to characterize the trade-off between model accuracy and efficiency far faster and more completely than previous approaches, which most often involve training multiple models.
- We use this to approach to demonstrate that our method enables choosing rescaling factors during inference based on rapidly computing an accuracy-efficiency trade-off for a dataset of interest. Since for various segmentation tasks a wide range of rescaling factors lead to similar final model accuracy, this offers the opportunity to substantially improve efficiency without sacrificing accuracy, enabling deployment in more resource-constrained settings, and lowering the energy requirements and carbon emissions of performing model inference.

- We show that learning a single model with varying rescaling factors has a regularization effect that makes networks trained using our method consistently more accurate than networks with a fixed rescaling factor.

2 Related Work

2.1 Resizing in Convolutional Neural Networks

Most modern CNNs are built from three main building blocks: learnable convolutional filters, normalization layers, and deterministic resizing layers to downscale or upscale feature maps [23, 55, 66, 79, 23]. Resizing layers have been implemented in a variety of ways, including max pooling, average pooling, bilinear sampling, and strided convolutions [2]. A common drawback of these pooling operations is that they enforce a fixed scale and receptive field on each resizing step. Pooling alternatives, such as strided and atrous convolutions [8, 9, 63] and learnable downsampling in the network [16], present the same limitation of operating at discrete integer steps.

Some alternative pooling approaches improve final model accuracy, such as combining max pooling and average pooling using learnable parameters [43, 72], pre-filtering features with antialiasing filters [74] or combining features at multiple resolutions [22]. These strategies focus on improving model accuracy and do not thoroughly study the efficiency aspect of the downsampling operations. Other methods have explored a wider range of rescaling operations by stochastically downsampling intermediate features [18, 42] leading to improvements to model generalization. Recent work has investigated differentiable resizing modules that replace pooling operations [35, 45], strided convolutions [57] or the resizing for preprocessing the input to the model [65]. These techniques optimize the differentiable modules as part of the training process, leading to improvements in model performance for a particular metric. In contrast, our goal is to efficiently learn many models with varying rescaling factors that characterize the entire trade-off curve between accuracy and efficiency. This allows users to choose at test time a model that appropriately balances efficiency and accuracy.

2.2 Hypernetworks

Hypernetworks are neural network models that output the weights for another neural network [19, 39, 60]. Hypernetworks have been used in a range of applications such as neural architecture search [7, 73], Bayesian optimization [41, 54], weight pruning [46], continual learning [67], multi-task learning [61] meta-learning [75] and knowledge editing [11]. Recent work has used hypernetworks to perform hyperparameter optimization [47, 49, 24, 69]. These gradient-based optimization approaches train a hypernetwork to predict the weights of a primary network conditioned on a hyperparameter value. Our work is also similar to hypernetwork based neural architecture search techniques in that both explore many potential architectures as a part of training [15]. However, we do not optimize the architectural properties of the network while training, instead we learn many architectures jointly.

3 Method

Convolutional neural networks (CNNs) are parametric functions $\hat{y} = f(x; \theta)$ that map input values x to output predictions \hat{y} using a set of learnable parameters θ . The network parameters θ are optimized to minimize a loss function \mathcal{L} given dataset \mathcal{D} using stochastic gradient descent strategies. For example, in supervised scenarios,

$$\theta^* = \arg \min_{\theta} \sum_{x, y \in \mathcal{D}} \mathcal{L}(f(x; \theta), y). \quad (1)$$

Most CNNs architectures use some form of rescaling layers with a *fixed* rescaling factor that rescale the intermediate network features, most often by halving (or doubling) along each spatial dimension.

We define a generalized version of convolutional models $f_{\varphi}(x, \theta)$ that perform feature rescaling by a *continuous* factor $\varphi \in [0, 1]$. Specifically, $f_{\varphi}(x; \theta)$ has the same parameters and operations as $f(x; \theta)$, with all intermediate feature rescaling operations being determined by the rescaling factor φ . Values of $\varphi = 1/2$ represent scaling by half as is prevalent in CNNs, lower values represent more aggressive rescaling, while values closer to 1 represent smaller spatial changes to the intermediate features.

Characterizing the model accuracy as a function of the rescaling factor φ for a particular dataset using standard techniques requires training multiple instances of $f_{\varphi}(\cdot; \theta)$, one for each rescaling factor, leading to substantial computational burden. We propose a framework where the family of parametric functions $f_{\varphi}(\cdot; \theta)$ is learned jointly, using an amortized learning strategy that learns the effect of rescaling factors φ on the network parameters θ . Motivated by work on hypernetworks, we employ a function $h(\varphi; \omega)$ with learnable parameters ω that maps the rescaling ratio φ to a set of

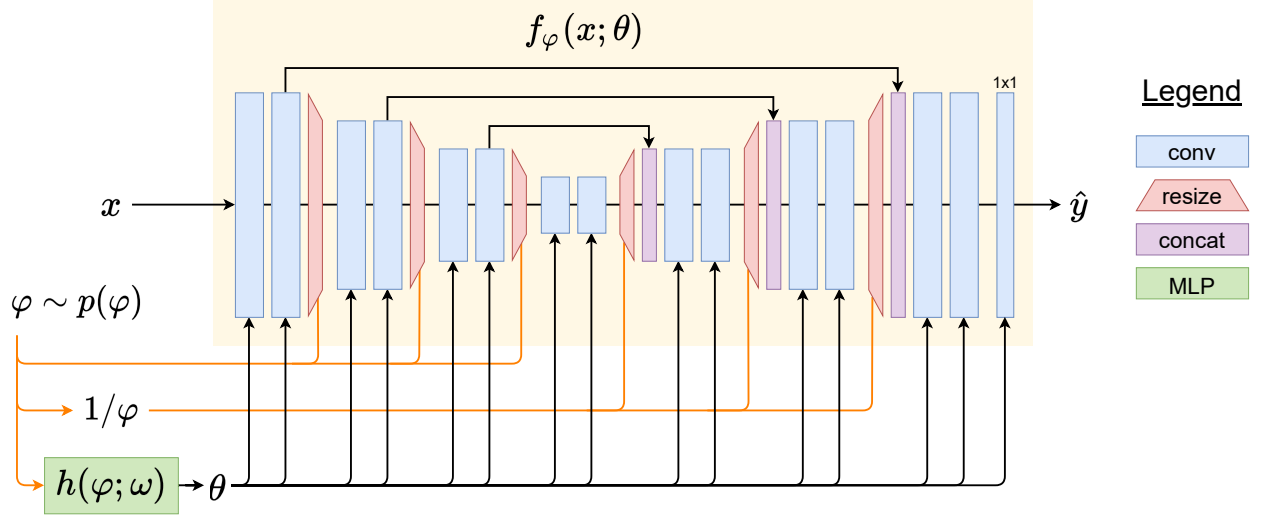


Figure 2: Diagram of the proposed hypernetwork-based model used to jointly learn a family of segmentation networks with flexible feature rescaling. At each iteration, a rescaling factor φ is sampled from a prior distribution $p(\varphi)$. Given φ , the hypernetwork $h(\varphi; \omega)$ predicts the parameter values θ of the primary network $f_\varphi(x; \theta)$. Given a sample datapoint x , we predict $\hat{y} = f_\varphi(x; \theta)$ and compute the loss $\mathcal{L}(\hat{y}, y)$ with respect to the true label y . The resulting loss gradients only lead to updates for learnable hypernetwork weights ω . The hypernetwork is implemented as a Multi Layer Perceptron (MLP) and the primary network uses a UNet-like architecture.

convolutional weights θ for the function $f_\varphi(\cdot; \theta)$. We model $h(\varphi; \omega)$ with another neural network, or *hypernetwork*, and optimize its parameters ω based on an amortized learning objective

$$\omega^* = \arg \min_{\omega} \sum_{x, y \in \mathcal{D}} \mathcal{L}(f_\varphi(x; h(\varphi; \omega)), y), \quad (2)$$

At each training iteration, we sample a resizing ratio $\varphi \sim p(\varphi)$ from a prior distribution $p(\varphi)$, which determines both the rescaling of internal representations and, via the hypernetwork, the weights of the primary network $f_\varphi(\cdot; \theta)$. Figure 2 presents the information flow between φ and the neural network models, where $f_\varphi(\cdot; \theta)$ illustrates the UNet-like architecture used in our experiments.

We highlight that even though the hypernetwork model has more trainable parameters than a regular primary network, the number of convolutional parameters θ is the same.

3.1 Rescaling Factor Selection

Once trained, the hypernetwork yields the convolutional parameters θ for any given input rescaling factor φ in a single forward pass. We examine two different ways to take advantage of this. First, we can exploit this landscape of models to rapidly select a rescaling factor φ under a new performance metric of interest on a held out set of data \mathcal{D}' that may be different from the training dataset. For example, we focus on inference computational cost, and devise a metric \mathcal{C} that captures the inference computational costs measurements, such as the number of floating point operations (FLOPs) or the peak memory consumption. We then solve the optimization problem

$$\begin{aligned} \varphi^* &= \arg \min_{\varphi} \mathcal{C}(f_\varphi(\cdot, h(\varphi; \omega), h) \\ \text{s.t. } &\text{Acc}(f_\varphi(\cdot, h(\varphi; \omega), \mathcal{D}') \geq \alpha, \end{aligned} \quad (3)$$

where $\text{Acc}(f_\varphi, \mathcal{D}')$ is an accuracy metric and α is a minimum desired accuracy. We can search for φ^* using black box hyperparameter search strategies such as random search, grid search, or tree Parzen estimators [3, 4]. The second way we exploit this landscape of models is to evaluate many values of φ to fully characterize the accuracy-efficiency Pareto frontier. This can be achieved efficiently since it does not involve any further training. In both cases, once φ^* is found, we leave out the hypernetwork entirely for inference purposes, using the predicted weights by the hypernetwork, thus incurring only the computational requirements of the primary CNN.

4 Experiments

We present two sets of experiments. The first set evaluates the accuracy and efficiency of segmentation models generated by our hypernetwork, both in absolute terms and relative to models generated with fixed resizing. Through the second set of experiments, we provide insights into the performance results.

4.1 Experimental Setup

Datasets. We use three widely-used segmentation datasets: OASIS, Caltech-UCSB Birds, and Oxford-IIIT Pets. OASIS is a medical imaging dataset containing 414 brain MRI scans that have been skull-stripped, bias-corrected, and resampled into an affinely aligned, common template space [24, 50]. For each scan, segmentation labels for 24 brain substructures in a 2D coronal slice are available. We split the data into 331 images for training and validation, and 83 images for test. The Oxford-IIIT Pet dataset [52] comprises 7,349 natural images (3,669 for training and validation, and 3,680 for test) from 37 species of domestic cats and dogs. Caltech-UCSD Birds-200-2011 [68] consists of 11,788 images (5994 for training and validation, and 5794 for test) from 200 bird species. Both CUBBirds and OxfordPets include segmentation maps. In all datasets, we trained using an 80%-20% train-validation split of the training data.

Segmentation Network. We use the UNet architecture, as it is the most prevalent and widely-used segmentation CNN architecture [58, 29]. We use bilinear interpolation layers to downsample or upsample a variable amount based on the hyperparameter φ for downsampling, or its inverse $1/\varphi$ for upsampling. We round the rescaled output size to the nearest integer to accommodate for discrete pixel sizes. We use five encoder stages and four decoder stages, with two convolutional operations per stage and LeakyReLU activations [48]. For networks trained on OASIS Brains we use 32 features at each convolutional filter weight. For the OxfordPets and CUBBirds datasets we use an encoder with (16, 32, 64, 128, 256) channels, and a decoder using (32, 16, 8, 4) channels at each stage respectively. We found that our results worked across various settings with many choices for the numbers of filters.

Hypernetwork. We implement the hypernetwork using three fully connected layers. Given a vector of $[\varphi, 1 - \varphi]$ as an input, the output size is set to the number of convolutional filters and biases in the segmentation network. We use the vector representation $[\varphi, 1 - \varphi]$ to prevent biasing the fully connected layers towards the magnitude of φ . The hidden layers have 10 and 100 neurons respectively and LeakyReLU activations [48] on all but the last layer, which has linear outputs. Hypernetwork weights are initialized using Kaiming initialization [21] with *fan out*, and bias vectors are initialized to zero.

Baseline Method. We train a set of conventional UNet models with fixed rescaling factors. These networks are identical to the primary network, but are trained without a hypernetwork and instead use a fixed ratio of φ . We train baseline models at 0.05 rescaling factor increments for the OASIS datasets from 0 to 1, and at 0.1 increments for the OxfordPets and CUBBirds datasets from 0 to 0.6.

Evaluation. We evaluate each segmentation method using the Dice score [12], which quantifies the overlap between two regions and is widely used in the segmentation literature. Dice is expressed as

$$\text{Dice}(y, \hat{y}) = \frac{2|y \cap \hat{y}|}{|y| + |\hat{y}|},$$

where y is the ground truth segmentation map and \hat{y} is the predicted segmentation map. A Dice score of 1 indicates perfectly overlapping regions, while 0 indicates no overlap. For datasets with more than one label, we average the Dice score across all foreground labels.

For each experimental setting we train five replicas with different random seeds and report mean and standard deviation. Once trained, we use the hypernetwork to evaluate a range of φ , using 0.01 intervals. This is more fine-grained than is feasible for the UNet baseline because all evaluations use the same model, whereas the UNet baseline requires training separate models for each rescaling factor.

Training. We train the networks using a categorical cross-entropy loss. We found alternative choices of loss function, such as a soft Dice-score loss, led to similar results in all tasks. We use the Adam optimizer [38] and train networks until the loss in the validation set stops improving. For networks trained on OASIS brains, we sample the rescaling hyperparameter φ from $\mathcal{U}(0, 1)$, and for the CUBBirds and OxfordPets datasets, we sample φ from the prior distribution $\mathcal{U}(0, 0.6)$. Because of the large number of features in the CUBBirds and OxfordPets models, we limit the prior so that the segmentation models do not exceed available GPU memory. We provide additional platform and reproducibility details in the appendix, and the code for our method is available at <https://github.com/JJGO/amortized-feature-scaling>.

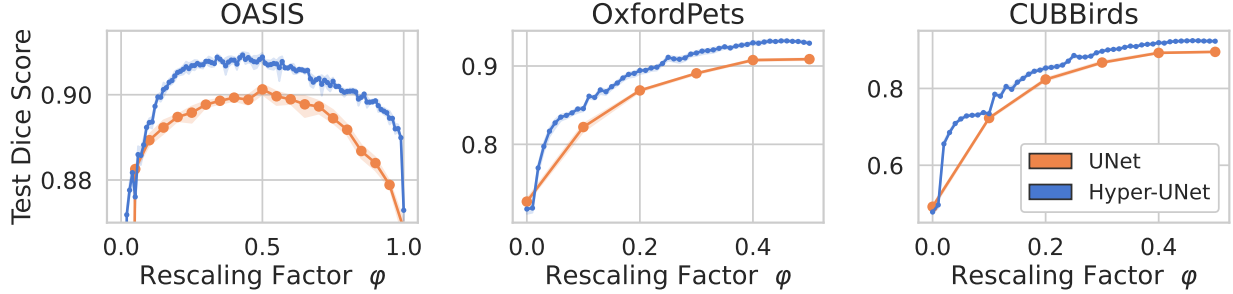


Figure 3: Comparison between a family of networks trained with fixed amounts of feature rescaling (UNet) and a single instance of the proposed hypernetwork method (Hyper-UNet) trained on the entire range of rescaling factors. We report results in the test set for the three considered segmentation datasets. In all settings the Hyper-UNet model outperforms the individually trained UNet models.

4.2 Accuracy and Computational Cost

4.2.1 Accuracy

First, we compare the accuracy of a single hypernetwork model (Hyper-UNet) to a set of baseline UNet models trained with fixed rescaling ratios. Our goal is to assess the ability of the hypernetwork model to learn a continuum of CNN weights for various rescaling factors, and evaluate how the performance of models using those weights compare to that of models trained independently with specific rescaling factors.

Figure 3 shows the Dice score on the held-out test split of each dataset as a function of the rescaling factor φ , for our approach and the baselines. We find that many rescaling factors can achieve similar final model performance, for example in the OASIS task, both strategies achieve a mean Dice score across brain structures above 0.89 for most rescaling factors. For the natural image datasets, we find that segmentation quality decreases more rapidly as φ decreases than for OASIS.

In all datasets, the networks predicted by the hypernetwork are consistently more accurate than equivalent networks trained with specific rescaling factors. The best rescaling factor found with the hypernetwork outperformed the best ratio for the UNet baseline by 0.8 Dice points on OASIS Brains, 3.1 Dice points in the OxfordPets dataset and 5 Dice points in the CUBBirds dataset. Experiments later in the paper delve deeper into this improvement in model generalization.

We also explore how varying the rescaling factor φ affects the segmentation of smaller labels in the image. Figure 4 presents a breakdown by neuroanatomical structures for a UNet baseline with $\varphi = 0.5$ and a subset of rescaling factors for the Hypernetwork model. We observe that the proposed hypernetwork model achieves similar performance for all labels regardless of their relative size, even when downsampling by substantially larger amounts than the baseline.

4.2.2 Computational Cost

We analyze how each rescaling factor affects the inference computational requirements of the segmentation networks by measuring the number of floating point operations (FLOPs) required to use the network for each rescaling factor at inference time. We also evaluate the amount of time used to train each model.

Figure 5 depicts the trade-off between test Dice score and the inference computational cost for both methods in all segmentation tasks. We observe that the choice of rescaling factor has a substantial effect on the computational requirements. For instance, for the OxfordPets and CUBBirds tasks, reducing the rescaling factor from the default $\varphi = 0.5$ to $\varphi = 0.4$ reduces computational cost by over 50% and by 70% for $\varphi = 0.3$. In all cases, we again find that hypernetwork achieves a better accuracy-FLOPs trade-off curve than the set of baselines. Tables 1 and 2 in the supplement report detailed measurements for accuracy (in Dice score), inference cost (in inference GFLOPs) and training time (in hours) for both approaches.

4.2.3 Efficiency Analysis

The hypernetwork-based approach facilitates examining the trade-off between computational efficiency and performance, as shown in Figure 5. As φ approaches 0, accuracy sharply drops as the amount of information that the UNet can propagate becomes extremely limited. As φ approaches 1, accuracy rapidly decreases as well, likely because with insufficient downsampling the network lacks spatial context to correctly perform the segmentation.

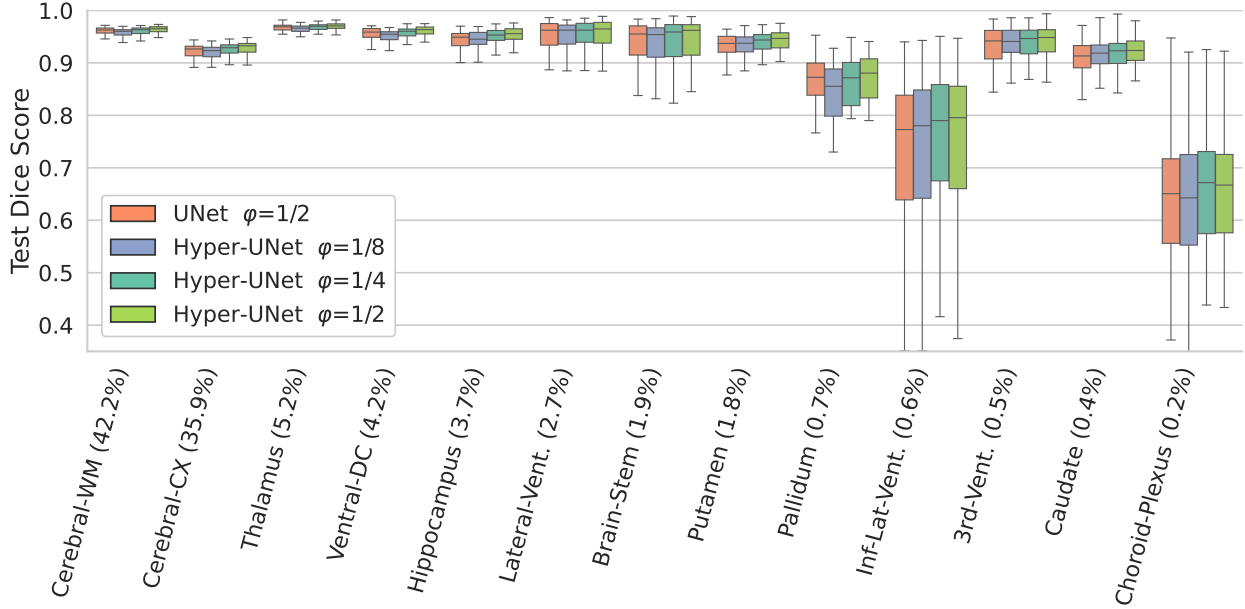


Figure 4: Segmentation Dice coefficient across various brain structures for the baseline method (UNet) trained and evaluated at $\varphi = 0.5$, and the hypernetwork approach evaluated at various rescaling factors φ (Hyper-UNet) for the OASIS test set. Anatomical structures are sorted by mean volume in the dataset (in parentheses). Labels consisting of left and right structures (e.g. Hippocampus) are combined. We abbreviate the labels: white matter (WM), cortex (CX) and ventricle (Vent). The proposed hypernetwork model achieves similar performance for all labels despite the reduction in feature map spatial dimensions for $\varphi = 0.5$.

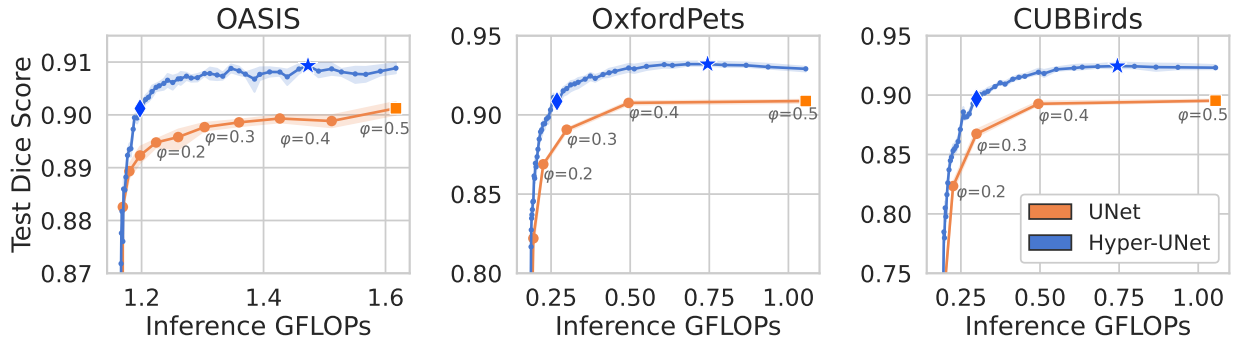


Figure 5: Trade-off curves between test model accuracy measured in Dice score and inference computational cost measured in GFLOPs for a family of networks trained with fixed amounts of feature rescaling (UNet) and for single instance of the proposed hypernetwork method (Hyper-UNet) trained on the entire range of rescaling factors. For all datasets, we find that most accurate model predicted by the hypernetwork (\star) outperforms the best baseline network while requiring fewer inference GFLOPs. Moreover, compared to the best UNet (\blacksquare), our method can achieve similar results (\blacklozenge), at a small fraction of the computational cost. Results are averaged across network initializations and variance is indicated with shaded regions.

Because of the identical cost of inference (for a given rescaling factor) and the improved segmentation quality of the hypernetwork models, the hypernetwork method Pareto curve dominates the regular networks, requiring less inference computation for comparable model quality. For example, for networks trained on OASIS, we observe that for $\varphi \in [0.25, 0.5]$ there is no loss in segmentation quality, showing that a more than 20% reduction in FLOPs can be achieved with no loss of performance. The hypernetwork achieves similar performance to the best baseline with $\varphi = 0.15$, while reducing the computational cost of inference by 26%.

The result is even more pronounced with the Oxford-Pets dataset. At $\varphi = 0.25$ the hypernetwork model matches the accuracy of the best baseline UNet while reducing the computational cost by 76%. Furthermore, going from a

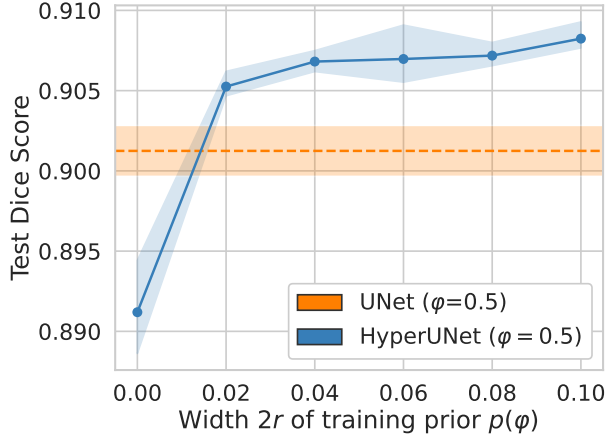


Figure 6: Test segmentation Dice on the OASIS Brains task as a function of the prior distribution range $2r$. Results are evaluated with $\varphi = 0.5$ in all settings, regardless of the training prior, and we also include a baseline UNet model. Uniform priors for φ are of the form $\mathcal{U}(0.5 - r, 0.5 + r)$, i.e. they linearly increase around 0.5. Standard deviation (shaded regions) is computed over 5 random initializations.

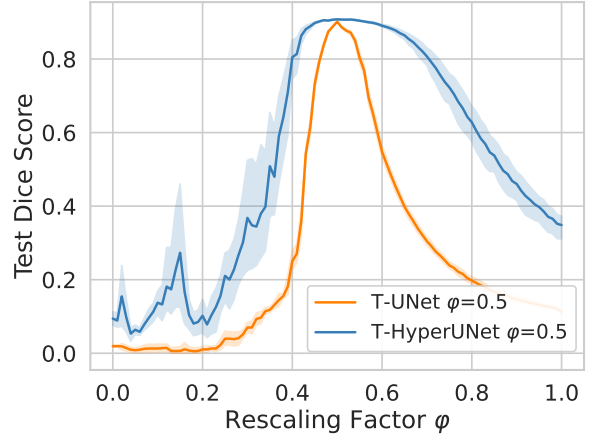


Figure 7: Segmentation results for models resulting from transferring weights learned for a given rescaling factor and evaluated at different factors. The convolutional parameters learned by the hypernetwork (T-Hyper) transfer to nearby factors substantially better than the weights of the baseline model (T-UNet). Standard deviation (shaded regions) is computed over 5 random seeds.

rescaling factor of $\varphi = 0.5$ to $\varphi = 0.25$ offers a 4x reduction in FLOPs with a 3 Dice point decrease. Characterizing the accuracy-efficiency Pareto frontier using our method requires substantially fewer GPU-hours than the traditional approach, while enabling a substantially more fine-scale curve. In our experiments, the set of baselines required over an order of magnitude ($10\times$) longer to train compared to the single hypernetwork model, even when we employ a coarse-grained baseline search. Had we done a more fine-grained search for the best ratio, we might have found a ratio that provided slightly better accuracy, but training would have required even more time. In practice, practitioners are rarely willing to train more than a few models. In contrast, we can instantiate our system at arbitrary values of φ without the need to retrain.

4.3 Analysis Experiments

In this section we perform additional experiments designed to shed light on why the hypernetwork models achieve higher test accuracy than the baseline UNet models.

4.3.1 Varying Prior Width

We first study the quality of hypernetwork segmentation results with varying width of the prior distribution $p(\varphi)$. Our goal is to understand how learning with varying amounts of rescaling affects segmentation accuracy and generalization. We train a set of hypernetwork models on the OASIS dataset but with narrow uniform distributions $\mathcal{U}(0.5 - r, 0.5 + r)$, where r controls the width of the distribution. We vary $r = [0, 0.01, \dots, 0.05]$ and evaluate them with $\varphi = 0.5$

Figure 6 shows Dice scores for training and test set on the OASIS segmentation task, as well as a baseline UNet for comparison. With $r = 0$, the hypernetwork is effectively trained with a constant $\varphi = 0.5$, and slightly underperforms compared to the baseline UNet. However, as the range of the prior distribution grows, the test Dice score of the hypernetwork models improves, surpassing the baseline UNet performance.

Figure 6 suggests that the improvement over the baselines can be at least partially explained by the hypernetwork learning a more robust model because it is exposed to varying amounts of feature rescaling. This suggests that stochastically changing the amount of downsampling at each iteration has a regularization effect on learning that leads to improvements in the model generalization. Wider ranges of rescaling values for the prior $p(\varphi)$ have a larger regularization effect. At high values of r , improvements become marginal and the accuracy of a model trained with the widest interval $p(\varphi) = \mathcal{U}(0.4, 0.6)$ is similar to the results of the previous experiments with $p(\varphi) = \mathcal{U}(0, 1)$.

4.3.2 Weight transferability.

We study the effect on segmentation results associated with using a set of weights that was trained with a different rescaling factor. Our goal is to understand how the hypernetwork adapts its predictions as the rescaling factor changes. We use *fixed* weights $\theta' = h(0.5; \omega)$ as predicted by the hypernetwork with input $\varphi' = 0.5$, and run inference using different rescaling factors φ . For comparison, we apply the same procedure to a set of weights of a UNet baseline trained with a fixed $\varphi = 0.5$.

Figure 7 presents segmentation results on OASIS for varying rescaling factors φ . Transferring weights from the baseline model leads to a rapid decrease in performance away from $\varphi = 0.5$. In contrast, the weights generated by the hypernetwork are more robust and can effectively be used in the range $\varphi \in [0.45, 0.6]$. Nevertheless, weights learned for a specific rescaling factor φ do not generalize well to a wide range of different rescaling factors, whereas weights predicted by the hypernetwork transfer substantially better to other rescaling factors.

5 Limitations

The proposed framework is designed for and evaluated on image segmentation, a prevalent task in computer vision and medical image analysis. We believe that it can be extended to other tasks like image registration or object detection. Constructing such extensions is an exciting area for future research.

When including rescaling factors $\varphi > 0.5$ as part of the prior, the proposed method has higher peak memory requirements than a regular UNet baseline (with $\varphi = 0.5$), which might require GPUs with larger memory capacity or model-parallel distributed training. The hypernetwork also introduces additional hyperparameters related to its architecture, such as the number of hidden neurons in each layer and the number of layers. While this is a complication, in our experiments, we found that many settings for these additional parameters led to similar results as those presented in the results.

We focus on the UNet as a benchmark architecture because it is a popular choice for segmentation networks across many domains [58, 14, 31, 28, 1, 5]. It also features key properties, such as an encoder-decoder structure and skip connections from the encoder to the decoder, that are used in other segmentation architectures [8, 77, 9]. Nevertheless, in Section C of the appendix, we report results for other popular segmentation architectures, including PSPNet, FPN and SENet. Our results indicate that our method is successful for those primary network architectures as well.

6 Summary

We introduce a hypernetwork-based approach for efficiently learning a family of CNNs with different rescaling factors in an amortized way.

Given a trained model, this proposed approach enables powerful downstream applications, such as efficiently generating the Pareto frontier for the trade-off between inference cost and accuracy. This makes it possible to rapidly search for a rescaling factor that maximizes model a new metric of interest at inference without retraining, such as maximizing accuracy subject to computational cost constraints. For example, using the hypernetwork, we demonstrate that using larger amounts of downsampling can often lead to a substantial reduction in the computational costs of inference, while sacrificing nearly no accuracy. Finally, we demonstrate that for a variety of image segmentation tasks, models learned with this method achieve accuracy at least as good, and more often better than, that of CNNs trained with fixed rescaling ratios, while producing more robust models. This strategy enables the construction of a new class of cost-adjustable models, which can be adapted to the resources of the user and minimize carbon footprint while providing competitive performance. We believe such models will substantially enable deployment of current machine learning systems across a variety of domains.

References

- [1] G. Balakrishnan, A. Zhao, M. R. Sabuncu, J. Guttag, and A. V. Dalca. Voxelmorph: a learning framework for deformable medical image registration. *IEEE transactions on medical imaging*, 38(8):1788–1800, 2019.
- [2] Y. Bengio, I. Goodfellow, and A. Courville. *Deep learning*, volume 1. MIT press Cambridge, MA, USA, 2017.
- [3] J. Bergstra and Y. Bengio. Random search for hyper-parameter optimization. *Journal of machine learning research*, 13(2), 2012.
- [4] J. Bergstra, R. Bardenet, Y. Bengio, and B. Kégl. Algorithms for hyper-parameter optimization. In *25th annual conference on neural information processing systems (NIPS 2011)*, volume 24. Neural Information Processing Systems Foundation, 2011.

- [5] B. Billot, D. N. Greve, K. Van Leemput, B. Fischl, J. E. Iglesias, and A. Dalca. A learning strategy for contrast-agnostic mri segmentation. In T. Arbel, I. Ben Ayed, M. de Bruijne, M. Descoteaux, H. Lombaert, and C. Pal, editors, *Proceedings of the Third Conference on Medical Imaging with Deep Learning*, volume 121 of *Proceedings of Machine Learning Research*, pages 75–93. PMLR, 06–08 Jul 2020. URL <https://proceedings.mlr.press/v121/billot20a.html>.
- [6] D. Blalock, J. J. G. Ortiz, J. Frankle, and J. Gutttag. What is the state of neural network pruning? *arXiv preprint arXiv:2003.03033*, 2020.
- [7] A. Brock, T. Lim, J. M. Ritchie, and N. Weston. Smash: one-shot model architecture search through hypernetworks. *arXiv preprint arXiv:1708.05344*, 2017.
- [8] L.-C. Chen, G. Papandreou, F. Schroff, and H. Adam. Rethinking atrous convolution for semantic image segmentation. *arXiv preprint arXiv:1706.05587*, 2017.
- [9] L.-C. Chen, Y. Zhu, G. Papandreou, F. Schroff, and H. Adam. Encoder-decoder with atrous separable convolution for semantic image segmentation. In *Proceedings of the European conference on computer vision (ECCV)*, pages 801–818, 2018.
- [10] F. Chollet. Xception: Deep learning with depthwise separable convolutions. In *Proceedings of the IEEE conference on computer vision and pattern recognition*, pages 1251–1258, 2017.
- [11] N. De Cao, W. Aziz, and I. Titov. Editing factual knowledge in language models. *arXiv preprint arXiv:2104.08164*, 2021.
- [12] L. R. Dice. Measures of the amount of ecologic association between species. *Ecology*, 26(3):297–302, 1945.
- [13] M. Drozdal, E. Vorontsov, G. Chartrand, S. Kadoury, and C. Pal. The importance of skip connections in biomedical image segmentation. In *International Workshop on Deep Learning in Medical Image Analysis, International Workshop on Large-Scale Annotation of Biomedical Data and Expert Label Synthesis*.
- [14] M. Drozdal, E. Vorontsov, G. Chartrand, S. Kadoury, and C. Pal. The importance of skip connections in biomedical image segmentation. In *Deep learning and data labeling for medical applications*, pages 179–187. Springer, 2016.
- [15] T. Elsken, J. H. Metzen, and F. Hutter. Neural architecture search: A survey. *The Journal of Machine Learning Research*, 20(1):1997–2017, 2019.
- [16] C. Etmann, R. Ke, and C.-B. Schönlieb. iunets: Fully invertible u-nets with learnable up-and downsampling. *arXiv preprint arXiv:2005.05220*, 2020.
- [17] T. Gale, E. Elsen, and S. Hooker. The state of sparsity in deep neural networks, 2019.
- [18] B. Graham. Fractional max-pooling. *arXiv preprint arXiv:1412.6071*, 2014.
- [19] D. Ha, A. Dai, and Q. V. Le. Hypernetworks. *arXiv preprint arXiv:1609.09106*, 2016.
- [20] S. Han, H. Mao, and W. J. Dally. Deep compression: Compressing deep neural network with pruning, trained quantization and huffman coding. In Y. Bengio and Y. LeCun, editors, *4th International Conference on Learning Representations, ICLR 2016, San Juan, Puerto Rico, May 2-4, 2016, Conference Track Proceedings*, 2016. URL <http://arxiv.org/abs/1510.00149>.
- [21] K. He, X. Zhang, S. Ren, and J. Sun. Delving deep into rectifiers: Surpassing human-level performance on imagenet classification. In *Proceedings of the IEEE international conference on computer vision*, pages 1026–1034, 2015.
- [22] K. He, X. Zhang, S. Ren, and J. Sun. Spatial pyramid pooling in deep convolutional networks for visual recognition. *IEEE transactions on pattern analysis and machine intelligence*, 37(9):1904–1916, 2015.
- [23] K. He, X. Zhang, S. Ren, and J. Sun. Deep residual learning for image recognition. In *Proceedings of the IEEE conference on computer vision and pattern recognition*, pages 770–778, 2016.
- [24] A. Hoopes, M. Hoffman, D. N. Greve, B. Fischl, J. Gutttag, and A. V. Dalca. Learning the effect of registration hyperparameters with hypermorph. *Machine Learning for Biomedical Imaging*, 1:1–30, 2022. ISSN 2766-905X. URL <https://melba-journal.org/2022:003>.
- [25] J. Hu, L. Shen, and G. Sun. Squeeze-and-excitation networks. In *Proceedings of the IEEE conference on computer vision and pattern recognition*, pages 7132–7141, 2018.
- [26] G. Huang, Z. Liu, L. Van Der Maaten, and K. Q. Weinberger. Densely connected convolutional networks. In *Proceedings of the IEEE conference on computer vision and pattern recognition*, pages 4700–4708, 2017.
- [27] I. Hubara, M. Courbariaux, D. Soudry, R. El-Yaniv, and Y. Bengio. Binarized neural networks. In *Proceedings of the 30th International Conference on Neural Information Processing Systems*, pages 4114–4122, 2016.

- [28] F. Isensee, J. Petersen, A. Klein, D. Zimmerer, P. F. Jaeger, S. Kohl, J. Wasserthal, G. Koehler, T. Norajitra, S. Wirkert, et al. nnu-net: Self-adapting framework for u-net-based medical image segmentation. *arXiv preprint arXiv:1809.10486*, 2018.
- [29] F. Isensee, P. F. Jaeger, S. A. Kohl, J. Petersen, and K. H. Maier-Hein. nnu-net: a self-configuring method for deep learning-based biomedical image segmentation. *Nature methods*, 18(2):203–211, 2021.
- [30] F. Isensee, P. F. Jaeger, S. A. Kohl, J. Petersen, and K. H. Maier-Hein. nnu-net: a self-configuring method for deep learning-based biomedical image segmentation. *Nature methods*, 18(2):203–211, 2021.
- [31] P. Isola, J.-Y. Zhu, T. Zhou, and A. A. Efros. Image-to-image translation with conditional adversarial networks. *CVPR*, 2017.
- [32] B. Jacob, S. Kligys, B. Chen, M. Zhu, M. Tang, A. Howard, H. Adam, and D. Kalenichenko. Quantization and training of neural networks for efficient integer-arithmetic-only inference. In *Proceedings of the IEEE Conference on Computer Vision and Pattern Recognition*, pages 2704–2713, 2018.
- [33] M. Jaderberg, A. Vedaldi, and A. Zisserman. Speeding up convolutional neural networks with low rank expansions. *arXiv preprint arXiv:1405.3866*, 2014.
- [34] S. A. Janowsky. Pruning versus clipping in neural networks. *Physical Review A*, 39(12):6600–6603, June 1989. ISSN 0556-2791. doi: 10.1103/PhysRevA.39.6600. URL <https://link.aps.org/doi/10.1103/PhysRevA.39.6600>.
- [35] C. Jin, R. Tanno, T. Mertzani, E. Panagiotaki, and D. C. Alexander. Learning to downsample for segmentation of ultra-high resolution images. *arXiv preprint arXiv:2109.11071*, 2021.
- [36] N. P. Jouppi, C. Young, N. Patil, D. Patterson, G. Agrawal, R. Bajwa, S. Bates, S. Bhatia, N. Boden, A. Borchers, et al. In-datacenter performance analysis of a tensor processing unit. In *Proceedings of the 44th Annual International Symposium on Computer Architecture*, pages 1–12. ACM, 2017.
- [37] A. Khan, A. Sohail, U. Zahoor, and A. S. Qureshi. A survey of the recent architectures of deep convolutional neural networks. *Artificial Intelligence Review*, 53(8):5455–5516, 2020.
- [38] D. P. Kingma and J. Ba. Adam: A method for stochastic optimization. *arXiv preprint arXiv:1412.6980*, 2014.
- [39] S. Klocek, Ł. Maziarka, M. Wołczyk, J. Tabor, J. Nowak, and M. Śmieja. Hypernetwork functional image representation. In *International Conference on Artificial Neural Networks*, pages 496–510. Springer, 2019.
- [40] A. Krizhevsky, I. Sutskever, and G. E. Hinton. Imagenet classification with deep convolutional neural networks. In *Advances in neural information processing systems*, pages 1097–1105, 2012.
- [41] D. Krueger, C.-W. Huang, R. Islam, R. Turner, A. Lacoste, and A. Courville. Bayesian hypernetworks. *arXiv preprint arXiv:1710.04759*, 2017.
- [42] J. Kuen, X. Kong, Z. Lin, G. Wang, J. Yin, S. See, and Y.-P. Tan. Stochastic downsampling for cost-adjustable inference and improved regularization in convolutional networks. In *Proceedings of the IEEE Conference on Computer Vision and Pattern Recognition*, pages 7929–7938, 2018.
- [43] C.-Y. Lee, P. W. Gallagher, and Z. Tu. Generalizing pooling functions in convolutional neural networks: Mixed, gated, and tree. In *Artificial intelligence and statistics*, pages 464–472. PMLR, 2016.
- [44] T.-Y. Lin, P. Dollár, R. Girshick, K. He, B. Hariharan, and S. Belongie. Feature pyramid networks for object detection. In *Proceedings of the IEEE conference on computer vision and pattern recognition*, pages 2117–2125, 2017.
- [45] S. Liu, Z. Lin, Y. Wang, J. Zhang, F. Perazzi, and E. Johns. Shape adaptor: A learnable resizing module. In *Proceedings of the European Conference on Computer Vision (ECCV)*, 2020.
- [46] Z. Liu, H. Mu, X. Zhang, Z. Guo, X. Yang, K.-T. Cheng, and J. Sun. Metapruning: Meta learning for automatic neural network channel pruning. In *Proceedings of the IEEE/CVF International Conference on Computer Vision*, pages 3296–3305, 2019.
- [47] J. Lorraine and D. Duvenaud. Stochastic hyperparameter optimization through hypernetworks. *arXiv preprint arXiv:1802.09419*, 2018.
- [48] A. L. Maas, A. Y. Hannun, and A. Y. Ng. Rectifier nonlinearities improve neural network acoustic models. In *Proc. icml*, volume 30, page 3. Citeseer, 2013.
- [49] M. MacKay, P. Vicol, J. Lorraine, D. Duvenaud, and R. Grosse. Self-tuning networks: Bilevel optimization of hyperparameters using structured best-response functions. *arXiv preprint arXiv:1903.03088*, 2019.

- [50] D. S. Marcus, T. H. Wang, J. Parker, J. G. Csernansky, J. C. Morris, and R. L. Buckner. Open access series of imaging studies (oasis): cross-sectional mri data in young, middle aged, nondemented, and demented older adults. *Journal of cognitive neuroscience*, 19(9):1498–1507, 2007.
- [51] O. Oktay, J. Schlemper, L. L. Folgoc, M. Lee, M. Heinrich, K. Misawa, K. Mori, S. McDonagh, N. Y. Hammerla, B. Kainz, et al. Attention u-net: Learning where to look for the pancreas. *arXiv preprint arXiv:1804.03999*, 2018.
- [52] O. M. Parkhi, A. Vedaldi, A. Zisserman, and C. V. Jawahar. Cats and dogs. In *IEEE Conference on Computer Vision and Pattern Recognition*, 2012.
- [53] D. A. Patterson, J. Gonzalez, Q. V. Le, C. Liang, L. Munguia, D. Rothchild, D. R. So, M. Texier, and J. Dean. Carbon emissions and large neural network training. *CoRR*, abs/2104.10350, 2021. URL <https://arxiv.org/abs/2104.10350>.
- [54] N. Pawłowski, A. Brock, M. C. Lee, M. Rajchl, and B. Glocker. Implicit weight uncertainty in neural networks. *arXiv preprint arXiv:1711.01297*, 2017.
- [55] I. Radosavovic, J. Johnson, S. Xie, W.-Y. Lo, and P. Dollár. On network design spaces for visual recognition. In *Proceedings of the IEEE International Conference on Computer Vision*, pages 1882–1890, 2019.
- [56] M. Rastegari, V. Ordonez, J. Redmon, and A. Farhadi. Xnor-net: Imagenet classification using binary convolutional neural networks. In *European conference on computer vision*, pages 525–542. Springer, 2016.
- [57] R. Riad, O. Teboul, D. Grangier, and N. Zeghidour. Learning strides in convolutional neural networks. In *International Conference on Learning Representations*, 2022. URL <https://openreview.net/forum?id=M752z9FKJP>.
- [58] O. Ronneberger, P. Fischer, and T. Brox. U-net: Convolutional networks for biomedical image segmentation. In *International Conference on Medical image computing and computer-assisted intervention*, pages 234–241. Springer, 2015.
- [59] L. Rundo, C. Han, Y. Nagano, J. Zhang, R. Hataya, C. Militello, A. Tangherloni, M. S. Nobile, C. Ferretti, D. Besozzi, et al. Use-net: Incorporating squeeze-and-excitation blocks into u-net for prostate zonal segmentation of multi-institutional mri datasets. *Neurocomputing*, 365:31–43, 2019.
- [60] J. Schmidhuber. A ‘self-referential’ weight matrix. In *International Conference on Artificial Neural Networks*, pages 446–450. Springer, 1993.
- [61] J. Serrà, S. Pascual, and C. Segura. Blow: a single-scale hyperconditioned flow for non-parallel raw-audio voice conversion. *arXiv preprint arXiv:1906.00794*, 2019.
- [62] N. Siddique, P. Sidike, C. Elkin, and V. Devabhaktuni. U-net and its variants for medical image segmentation: theory and applications. *arXiv preprint arXiv:2011.01118*, 2020.
- [63] J. T. Springenberg, A. Dosovitskiy, T. Brox, and M. Riedmiller. Striving for simplicity: The all convolutional net. *arXiv preprint arXiv:1412.6806*, 2014.
- [64] V. Sze, Y.-H. Chen, T.-J. Yang, and J. Emer. Efficient processing of deep neural networks: A tutorial and survey. *arXiv preprint arXiv:1703.09039*, 2017.
- [65] H. Talebi and P. Milanfar. Learning to resize images for computer vision tasks. In *Proceedings of the IEEE/CVF International Conference on Computer Vision (ICCV)*, pages 497–506, October 2021.
- [66] M. Tan and Q. V. Le. Efficientnet: Rethinking model scaling for convolutional neural networks. *arXiv preprint arXiv:1905.11946*, 2019.
- [67] J. von Oswald, C. Henning, J. Sacramento, and B. F. Grewe. Continual learning with hypernetworks. *arXiv preprint arXiv:1906.00695*, 2019.
- [68] C. Wah, S. Branson, P. Welinder, P. Perona, and S. Belongie. The Caltech-UCSD Birds-200-2011 Dataset. Technical Report CNS-TR-2011-001, California Institute of Technology, 2011.
- [69] A. Q. Wang, A. V. Dalca, and M. R. Sabuncu. Hyperrecon: Regularization-agnostic cs-mri reconstruction with hypernetworks. In *Machine Learning for Medical Image Reconstruction: 4th International Workshop, MLMIR 2021, Held in Conjunction with MICCAI 2021, Strasbourg, France, October 1, 2021, Proceedings 4*, pages 3–13. Springer, 2021.
- [70] S. Xie, R. Girshick, P. Dollár, Z. Tu, and K. He. Aggregated residual transformations for deep neural networks. In *Proceedings of the IEEE conference on computer vision and pattern recognition*, pages 1492–1500, 2017.
- [71] T.-J. Yang, Y.-H. Chen, and V. Sze. Designing energy-efficient convolutional neural networks using energy-aware pruning. In *Proceedings of the IEEE Conference on Computer Vision and Pattern Recognition*, pages 5687–5695, 2017.

- [72] D. Yu, H. Wang, P. Chen, and Z. Wei. Mixed pooling for convolutional neural networks. In *International conference on rough sets and knowledge technology*, pages 364–375. Springer, 2014.
- [73] C. Zhang, M. Ren, and R. Urtasun. Graph hypernetworks for neural architecture search. *arXiv preprint arXiv:1810.05749*, 2018.
- [74] R. Zhang. Making convolutional networks shift-invariant again. In *International Conference on Machine Learning*, pages 7324–7334. PMLR, 2019.
- [75] D. Zhao, J. von Oswald, S. Kobayashi, J. Sacramento, and B. F. Grewe. Meta-learning via hypernetworks. 2020.
- [76] H. Zhao, J. Shi, X. Qi, X. Wang, and J. Jia. Pyramid scene parsing network. In *Proceedings of the IEEE conference on computer vision and pattern recognition*, pages 2881–2890, 2017.
- [77] H. Zhao, J. Shi, X. Qi, X. Wang, and J. Jia. Pyramid scene parsing network. In *Proceedings of the IEEE conference on computer vision and pattern recognition*, pages 2881–2890, 2017.
- [78] Z. Zhong, Z. Q. Lin, R. Bidart, X. Hu, I. B. Daya, Z. Li, W.-S. Zheng, J. Li, and A. Wong. Squeeze-and-attention networks for semantic segmentation. In *Proceedings of the IEEE/CVF conference on computer vision and pattern recognition*, pages 13065–13074, 2020.
- [79] B. Zoph, V. Vasudevan, J. Shlens, and Q. V. Le. Learning transferable architectures for scalable image recognition. In *Proceedings of the IEEE conference on computer vision and pattern recognition*, pages 8697–8710, 2018.

A Experimental Setup

A.1 Implementation Details

We provide additional implementation details:

Architecture. To bridge the mismatch between continuous rescaling factor φ values and discrete spatial dimensions in the feature maps, we round the spatial dimensions of the outputs of downscaling operations to the nearest integer value. For upscaling operations we use $1/\varphi$ but round the upscaled spatial dimensions so that they match the dimensions of the features from the skip connections used in the concatenation. We use a final convolution, with kernel size 1x1 and without activation function, to transform the number of channels to the target number of labels for the segmentation task.

Batch Size. Networks trained using the OASIS Brains dataset use a batch size of 8, whereas for networks trained on CUBBirds and OxfordPets datasets we use a batch size of 32 samples due to GPU memory constraints. For efficient training, we use the same φ value for the entire minibatch of samples. While in principle it is possible to use separate φ values within the same minibatch, this leads to intermediate features in the minibatch having different spatial dimensions, which substantially slows down training as vectorized operations cannot be used.

Initialization. We separate the weights of the last fully connected layer of the hypernetwork into different groups, each one corresponding to a fully connected layer predicting an individual parameter tensor of the primary network. This strategy leads to each predicted parameter of the primary network having an initialization that only depends on its own dimensions and not on the entire architecture.

Data Augmentation. We train using data augmentation on the CUBBirds and OxfordPets datasets, performing random resized crops and random horizontal flips. For the test set we do not perform any form of data augmentation.

Training. We use the Adam optimizer with default β parameters $\beta_1 = 0.9$ and $\beta_2 = 0.99$. For training we include a label for the background to ensure the cross-entropy loss has exactly one label for each pixel in the output. We do not use the background label when computing evaluation metrics.

Table 1: Segmentation performance on the OASIS Brains dataset in terms of mean Dice score for a held-out test set, across five random seeds, as well as the corresponding computational cost of running inference (in GFLOPs) and the required training time in hours. We highlight hypernet models with the best segmentation results and those with the smallest computational cost that perform comparably to the best UNet baseline

Model	φ	Dice (std)	Gflops	Train Time (h)
UNet	0.05	0.883 (0.001)	1.169	0.26
	0.10	0.889 (0.002)	1.180	0.27
	0.15	0.892 (0.002)	1.197	0.27
	0.20	0.895 (0.001)	1.224	0.28
	0.25	0.896 (0.002)	1.260	0.28
	0.30	0.898 (0.001)	1.303	0.29
	0.35	0.899 (0.001)	1.360	0.30
	0.40	0.899 (0.001)	1.427	0.31
	0.45	0.899 (0.001)	1.512	0.33
	0.50	0.901 (0.002)	1.617	0.35
	0.55	0.900 (0.002)	1.733	0.38
	0.60	0.899 (0.001)	1.882	0.41
	0.65	0.898 (0.003)	2.048	0.44
	0.70	0.897 (0.002)	2.256	0.49
	0.75	0.894 (0.002)	2.510	0.54
	0.80	0.892 (0.002)	2.787	0.60
	0.85	0.887 (0.002)	3.128	0.68
0.90	0.884 (0.002)	3.518	0.76	
0.95	0.879 (0.001)	3.991	0.86	
Hypernetwork	0.05	0.876 (0.003)	1.169	
	0.10	0.893 (0.001)	1.180	
	0.15	0.901 (0.002)	1.197	
	0.20	0.905 (0.001)	1.224	
	0.25	0.907 (0.001)	1.260	
	0.30	0.908 (0.001)	1.303	
	0.35	0.909 (0.001)	1.360	
	0.40	0.908 (0.001)	1.427	
	0.45	0.909 (0.001)	1.512	
	0.50	0.909 (0.001)	1.617	0.64
	0.55	0.907 (0.001)	1.733	
	0.60	0.907 (0.001)	1.882	
	0.65	0.906 (0.001)	2.048	
	0.70	0.904 (0.001)	2.256	
	0.75	0.903 (0.001)	2.510	
	0.80	0.901 (0.001)	2.787	
	0.85	0.899 (0.001)	3.128	
0.90	0.899 (0.000)	3.518		
0.95	0.894 (0.002)	3.991		

B Additional Results

Table 2: Segmentation performance on the OxfordPets and CUBBirds datasets in terms of mean Dice score for a held-out test set, across five random seeds, as well as the corresponding computational cost of running inference (in GFLOPs) and the required training time in hours. We highlight hypernet models with the best segmentation results and those with the smallest computational cost that perform comparably to the best UNet baseline

Dataset	Model	φ	Dice (std)	Gflops	Train Time (h)
OxfordPets	UNet	0.1	0.822 (0.005)	0.194	1.17
		0.2	0.869 (0.002)	0.225	1.28
		0.3	0.891 (0.001)	0.299	1.50
		0.4	0.908 (0.001)	0.495	2.14
		0.5	0.909 (0.001)	1.055	3.08
		0.6	0.899 (0.001)	2.381	5.95
	Hypernetwork	0.05	0.827 (0.006)	0.187	
		0.10	0.846 (0.003)	0.194	
		0.15	0.874 (0.003)	0.206	
		0.20	0.894 (0.004)	0.225	
		0.25	0.911 (0.004)	0.258	
		0.30	0.917 (0.003)	0.299	5.4
		0.35	0.925 (0.002)	0.374	
		0.40	0.930 (0.003)	0.495	
		0.45	0.932 (0.001)	0.683	
		0.50	0.929 (0.002)	1.055	
		0.55	0.924 (0.002)	1.550	
		0.60	0.916 (0.003)	2.381	
CUBBirds	UNet	0.1	0.723 (0.003)	0.194	2.20
		0.2	0.823 (0.004)	0.225	2.47
		0.3	0.867 (0.003)	0.299	2.96
		0.4	0.893 (0.002)	0.495	3.98
		0.5	0.895 (0.001)	1.055	6.22
		0.6	0.873 (0.003)	2.381	11.03
	Hypernetwork	0.05	0.721 (0.003)	0.187	
		0.10	0.734 (0.004)	0.194	
		0.15	0.816 (0.005)	0.206	
		0.20	0.853 (0.005)	0.225	
		0.25	0.886 (0.005)	0.258	
		0.30	0.897 (0.002)	0.299	10.3
		0.35	0.910 (0.002)	0.374	
		0.40	0.919 (0.003)	0.495	
		0.45	0.924 (0.002)	0.683	
		0.50	0.923 (0.002)	1.055	
		0.55	0.915 (0.003)	1.550	
		0.60	0.902 (0.003)	2.381	

C Additional Experiments

Segmentation Architecture Ablation Experiment

We originally tested our method on using the U-Net architecture [58], which is a popular architecture choice in image segmentation tasks, particularly for medical imaging applications [30]. Nevertheless, our method can be extended to other architectures. Given an arbitrary segmentation network, our method requires replacing fixed resizing layers with variable resizing layers and using the hypernetwork to predict all the convolutional parameters of the network.

In this experiment we test our method on other popular alternative segmentation architectures. While the majority of segmentation architectures feature the same basic components (convolutional layers, resizing layers, skip connections), we aimed to cover other architectural components not included in the U-Net design such as pyramid spatial pooling layers and squeeze-excitation layers. The ablation includes the following architectures:

- **Residual UNet.** This is popular U-Net variant where the operations at each resolution feature a residual connection similar to the ResNet architecture [62]. Previous work has highlighted the importance of this type of connections in biomedical image segmentation [13].
- **FPN.** Feature Pyramid Networks [44] construct a pyramid of features at several resolution levels, combining them in a fully convolutional manner and performing predictions at multiple resolutions during training.
- **PSPNet.** Pyramid Spatial Pooling [76] layers gather context information at multiple resolution levels in parallel, and several competitive natural image segmentation models include them in their architectures [9]. For our implementation, we perform the dynamic resizing operations in the encoder part and used the multi resolution PSP blocks in the decoder part.
- **SENet.** Squeeze Excitation networks [25] incorporate an attention mechanism to dynamically reweigh feature map channels during the forward pass. Squeeze-Excitation layers have been shown to be performant in segmentation tasks [78, 51, 59]. In our implementation, we include Squeeze-Excitation layers to both the encoder and the decoder stages of the network.

For each considered architecture we compare a single hypernetwork with a variable rescaling factor to a set of individual baselines with varying rescaling factors. We train baselines at 0.05 φ increments, i.e. $\varphi = 0, 0.05, 0.1, \dots, 1$. For the hypernetwork model we sample from $p(\varphi) = \mathcal{U}(0, 1)$. We evaluate on the OASIS2d semantic segmentation task introduced in the paper, which features 24 brain structure labels. We evaluate using Dice score and average over the labels. Results in Figure 8 show segmentation quality as the rescaling factor φ varies. We find similar results to those in the paper (Figure 3) with our single hypernetwork model matching the set of individually trained networks.

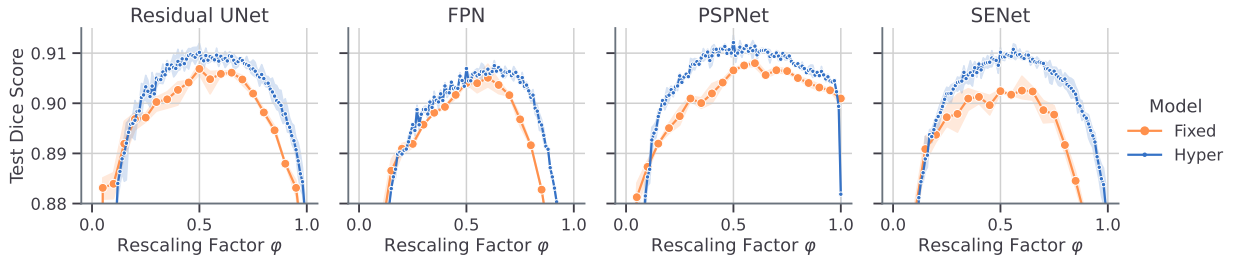


Figure 8: **Segmentation Architecture Ablation** Test Dice Score on the OASIS segmentation task for various choices of primary network architecture. Each plot features a family of networks trained with fixed amounts of feature rescaling (Fixed) and a single instance of the proposed hypernetwork method (Hyper) trained on the entire range of rescaling factors. Results are averaged across three random initializations, and the shaded regions indicate the standard deviation across them.

Variable Resolution Baseline Experiment

We compared our method to other networks with fixed rescaling factors φ . An alternative baseline involves training a regular model with $\varphi = 0.5$ and stochastically changing the resolution of the input images and segmentation labels during training. By exposing the model to multiple resolutions during training, we can then vary the input resolution at inference, providing a Quality-FLOPS trade-off.

Variable Resolution U-Net. We train a U-Net model equivalent to those in the paper with $\varphi = 0.5$. During training, at each training step the input is resized a factor $r \sim \mathcal{U}[0, 1]$, and the network output is resized by a factor of $1/r$. At inference, we sweep the values of $r \in [0, 1]$ to characterize the Pareto accuracy-efficiency curve.

Variable Resolution Hyper-UNet. We also consider a variable-resolution variant of our hypernetwork model where the input is rescaled by the a factor of φ and the prediction is rescaled by a factor of $1/\varphi$

We evaluate on the OASIS2d semantic segmentation task introduced in the paper, which features 24 brain structure labels. We evaluate using Dice score and average over the labels.

Figure 9 shows trade-off curves for the hypernetwork method, the set of fixed rescaling baselines, the variable-resolution baseline, and the variable-resolution hypernetwork model. We observe that both the variable-resolution baseline and hypernetwork model present substantially worse segmentation results to the methods evaluated in the paper. At the same time, the variable resolution methods explore a wider range of inference costs as they do not perform the outermost convolutional operations at full resolution. For the inference costs where the hypernetwork method is defined, it dominates all other approaches.

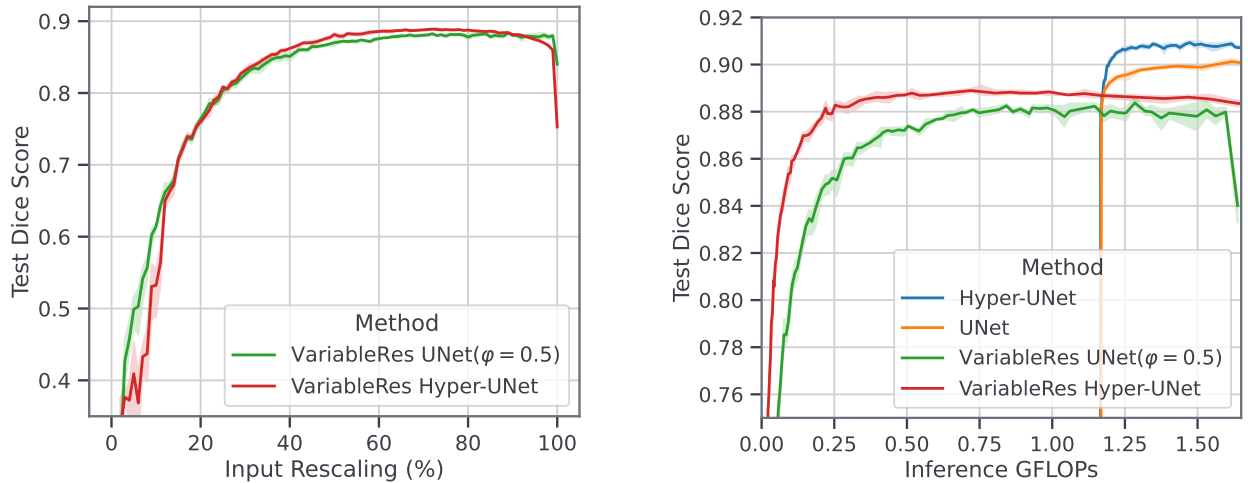


Figure 9: **Segmentation Architecture Ablation (Left)** Segmentation Dice coefficient for models trained with variable resolution inputs. **(Right)** Trade-off curves between test model accuracy measured in Dice score and inference computational cost measured in GFLOPs. Results include a variable-resolution UNet model with rescaling factor $\varphi = 0.5$ trained with variable resolutions (VariableRes UNet($\varphi = 0.5$)), as well as a hypernetwork model trained in a similar fashion (VariableRes Hyper-UNet). We also include the main hypernetwork method (Hyper-UNet) and the set of fixed rescaling baselines (UNet). Results are averaged across three random initializations, and the shaded regions indicate the standard deviation across them.

C.1 Separate Rescaling Factors

In the main body of the paper, we explored using a single rescaling factor φ to control all rescaling operations in the network. In this section, we also study a more general formulation where each downscaling step is controlled by a separate rescaling factor φ_i . Our experiments show that a hypernetwork model is capable of modeling this hyperparameter space despite the increased dimensionality. We find that this more general formulation achieves comparable accuracy and efficiency to the single rescaling factor model, with similar accuracy-efficiency Pareto frontiers.

Method. We use separate factors $\varphi = \{\varphi_0, \varphi_1, \dots, \varphi_K\}$ for each rescaling operation in the network. We train the hypernetwork $h(\varphi; \omega)$ to predict the set of weights θ for a set of rescaling factors φ . For a network with K downscaling and K upscaling steps, the rescaling factor φ_i controls both the downscaling of the i^{th} block of the network and the upscaling of the $(K - i)^{\text{th}}$ upscaling block to achieve consistent spatial dimensions between the respective encoder and decoder. Figure 10 presents a diagram of the flow of information for the case of a UNet with four levels and three rescaling steps.

Setup. We train the hypernetwork model on the OASIS segmentation task using the same experimental setup as the single rescaling factor experiments. We sample each $\varphi_i \sim \mathcal{U}(0, 1)$ independently. We use the same $(\varphi_i, 1 - \varphi_i)$ input encoding to prevent biasing the predicted weights towards the magnitude of the input values. Once trained, we evaluate

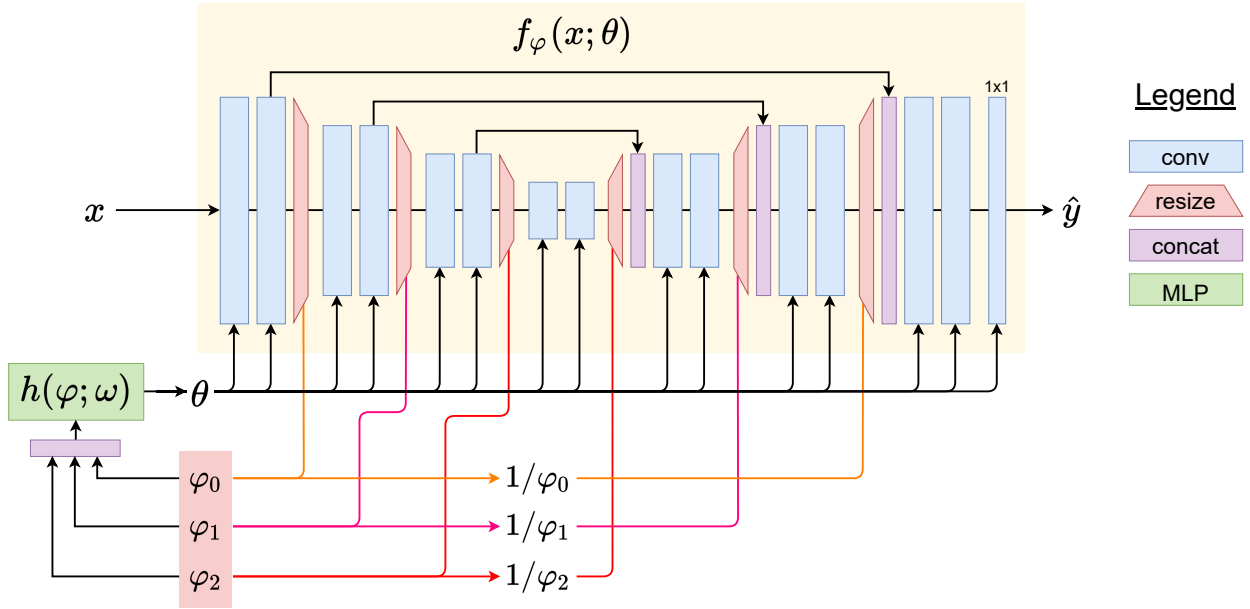


Figure 10: Diagram for the hypernetwork based model with multiple separate rescaling factors $(\varphi_0, \varphi_1, \varphi_2)$. Each rescaling factor φ_i determines the downscaling and upscaling of the i^{th} downscaling step and the i^{th} to last upscaling step. Given a series of rescaling factor values φ , the hypernetwork $h(\varphi; \omega)$ predicts the parameter values θ of the primary segmentation network $f_\varphi(x; \theta)$.

using the test set, sampling each of the three rescaling factors by 0.1 increments. This amounts to $11^3 = 1331$ different settings.

Results. Figure 11 shows Dice scores for the OASIS test set as we vary each of the rescaling factors φ in the network. The hypernetwork is capable of achieving high segmentation accuracy (> 0.88 dice points) for the vast majority of $\varphi = (\varphi_0, \varphi_1, \varphi_2)$ settings. Figure 12 shows the trade-off between segmentation accuracy and inference cost for the evaluated settings of φ along with the baseline and the hypernetwork model with a single rescaling factor.

Discussion. We find that first rescaling factor φ_0 has the most influence of segmentation results, while φ_2 has the least. The model achieves optimal results when $\varphi_0 \in [0.3, 0.5]$. We observe that as either φ_0 or φ_1 approach zero, segmentation accuracy sharply drops, consistent with the behavior we found in the networks with a common rescaling factor. Having separate rescaling factors φ yields results comparable to using a single factor φ for the whole network.

We highlight that $h(\varphi; \omega)$ manages to learn a higher dimensional hyperparameter input space successfully using the same model capacity. Moreover, we find that for the vast majority of φ settings the segmentation accuracy is quite high for the segmentation task, suggesting that the task can be solved with a wide array of rescaling settings. In Figure 12 we show that despite the increased hyperparameter space the Pareto frontier closely matches the results of using a single rescaling factor, suggesting that having a single rescaling factor is a good choice for this task.

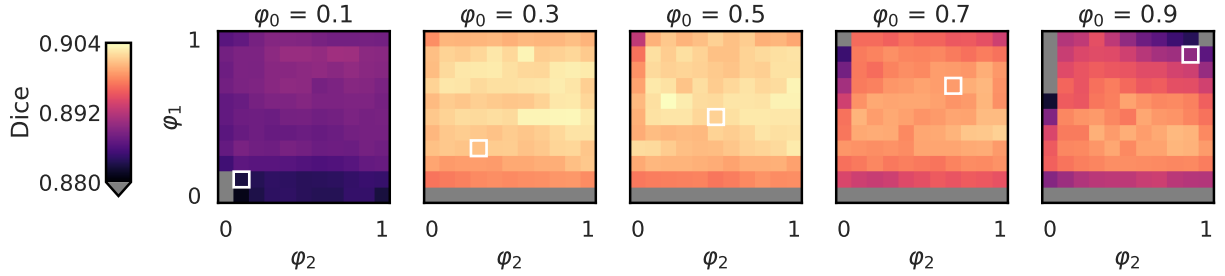


Figure 11: Segmentation results on a hypernetwork model with separate factors $\varphi = (\varphi_0, \varphi_1, \varphi_2)$ for each rescaling operation in the segmentation network. We report mean dice score across all anatomical structures on the OASIS test set. We highlight in white the φ settings explored by our single factor model. We mask underperforming settings (<0.88) with grey to maximize the dynamic range of the color map. We find that the first rescaling factor φ_0 has a substantially larger influence in segmentation quality compared to φ_1 and φ_2 .

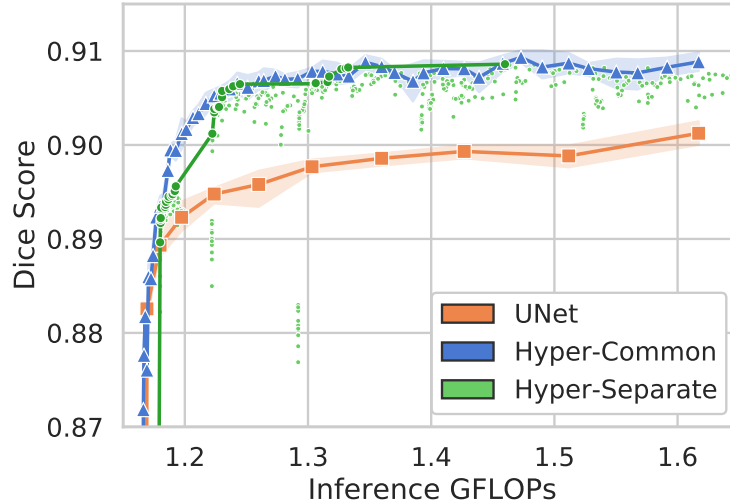


Figure 12: Segmentation accuracy as a function of required GFLOPs for one inference pass in the network. Mean Dice score across all anatomical structures on the OASIS test set for the baseline models (UNet), the hypernetwork model with a common rescaling factor φ (Hyper-Common), and the hypernetwork model with separate rescaling factors $(\varphi_0, \varphi_1, \varphi_2)$. For Hyper-Separate we include both individual suboptimal points and the Pareto frontier as a line.

D Additional Analysis

We include additional visualizations of how varying the rescaling factor φ affects the predicted weights and the associated feature maps. Figure 14 illustrates the predicted network parameters for a series of channels and layers as the rescaling factor φ varies. To capture the variability of the predicted parameters, Figure 13 presents the coefficient of variation for parameters across a series of rescaling factors. We observe that the first layer presents little to no variation as φ changes. Figure 15 presents sample feature maps as the rescaling factor φ changes, for separate layers in the network. The predicted convolutional kernels by the hypernetwork extract similar anatomical regions for different values of φ .

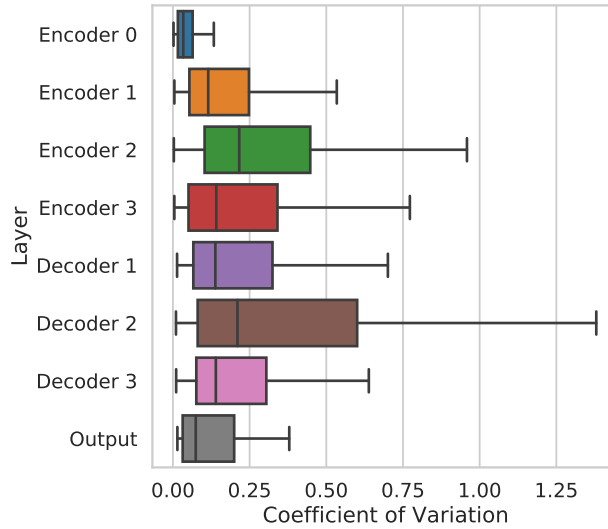


Figure 13: Coefficient of variation (CV) ($\sigma/|\mu|$) for each convolutional parameter predicted by the hypernetwork across a series of rescaling ratios $\varphi = \{0, 0.1, 0.2, \dots, 1.0\}$. Features at the first layer and the last layer present substantially smaller CV values compared to the rest of the layers.

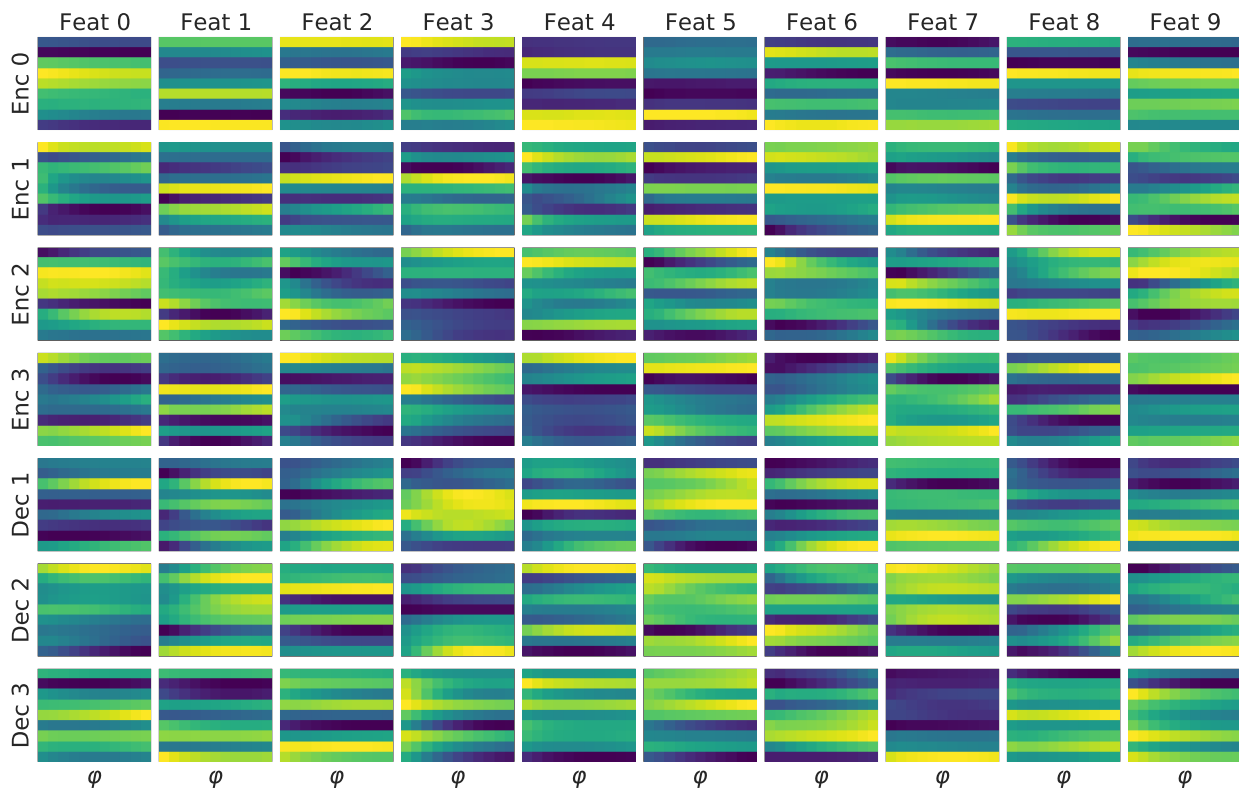


Figure 14: Sample predicted convolutional parameters maps for various features channels (columns) and for different primary network layers (rows). For each feature we show how each convolutional parameter (y-axis) changes as the rescaling factor φ varies (x-axis). We find that the hypernetwork leads to substantial variability as φ changes in some layers, especially those near the middle of the architecture.

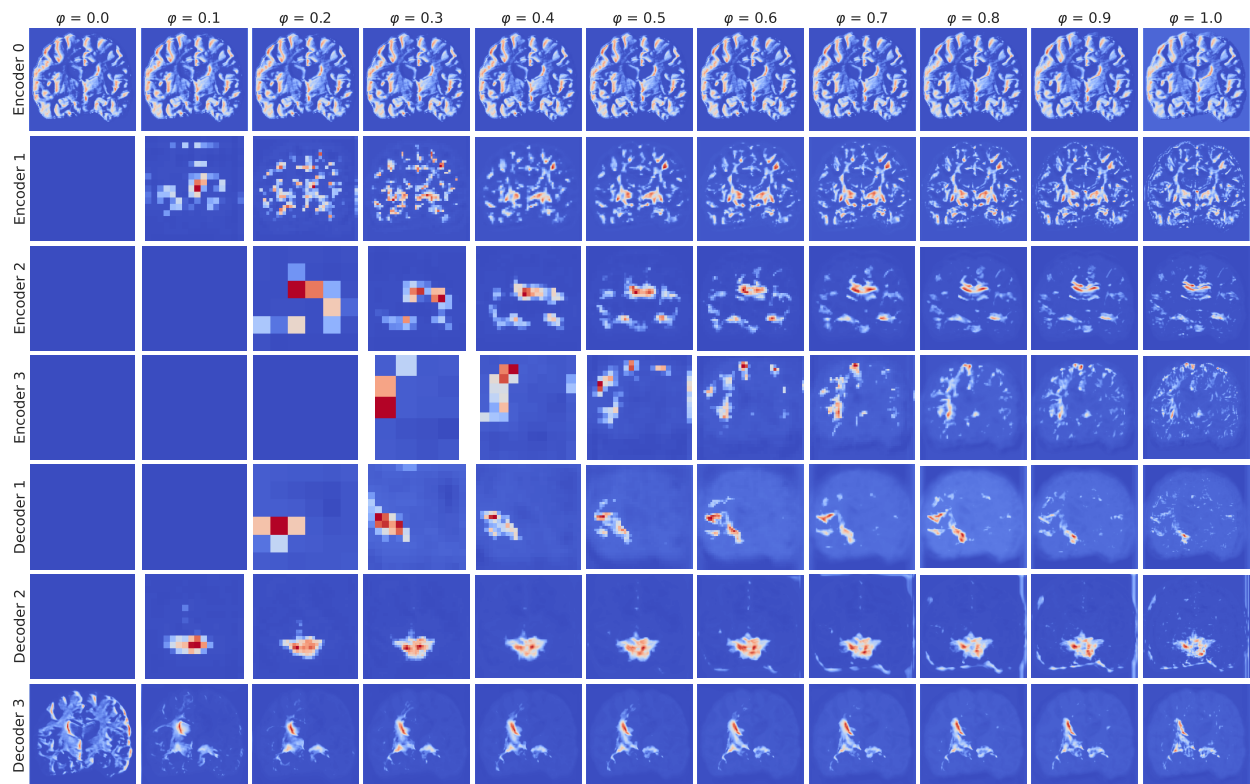


Figure 15: Sample intermediate convolutional feature maps for various rescaling factors φ (columns) and different primary network layers (rows).